

First CMS results at 13 TeV

P. Ronchese^{1,*}

on behalf of the CMS Collaboration

¹*INFN and University of Padova, Italy*

Abstract. Measurements of b -hadron and quarkonium production cross sections provide essential information to understand QCD. This talk will show new measurements of double-differential production cross sections vs. transverse momentum p_T and rapidity y , at center-of-mass energy $\sqrt{s} = 13$ TeV, performed by CMS experiment with data collected in 2015. Comparisons with results obtained at $\sqrt{s} = 7$ TeV will be shown.

1 Introduction

The motivations to study heavy flavour physics at CMS [1] include the probe of the underlying QCD processes, obtained by measuring b -hadron production cross-section and quarkonium polarization and by looking for new and exotic states. The measurements of the production cross-section for B^+ mesons and ψ, Υ quarkonia from CMS at a center of mass energy $\sqrt{s} = 13$ TeV will be shown.

2 The CMS experiment

The main components of the CMS experiment [1] are the tracker with pixels and microstrips, the electromagnetic and hadron calorimeters, and the muon detectors. Three different detectors are dedicated to muon trigger and detection, having the capability to perform a standalone reconstruction of muons. The match between the reconstruction from the tracker and the muon detectors can be conducted inside-out, that is more efficient at low transverse momentum, or outside-in, that is more efficient at high p_T . The misidentification probability is less than 1% and the momentum resolution ranges from 1% to 6% for muons up to 100 GeV.

Muons play an essential role in triggering events in the harsh LHC environment, characterized by a very high luminosity, while keeping the frequency inside a limited bandwidth. Triggers for B physics require the presence of two muons at least, possibly together with an additional track. The trigger system consists of a first level, based on a dedicated hardware taking fast decision and giving a trigger rate of the order of ~ 100 kHz, followed by an higher level based on software performing full track reconstruction and giving a rate of ~ 1 kHz. Specific triggers have been developed for different analyses, applying cuts on muon and dimuon transverse momentum and rapidity, the presence of secondary vertices and their displacement from the interaction point, the dimuon mass and the angle formed by the dimuon momentum and the flight direction, given by the position of the secondary

*e-mail: paolo.ronchese@pd.infn.it

vertex relative to the collision point. In the first year of run at $\sqrt{s} = 13$ TeV LHC delivered an integrated luminosity $\mathcal{L} \sim 4 \text{ fb}^{-1}$, and CMS recorded data corresponding to $\mathcal{L} \simeq 3.6 \text{ fb}^{-1}$. For muon-based analyses an integrated luminosity $\mathcal{L} \simeq 2.7 \text{ fb}^{-1}$ was collected.

3 Double Υ production

In the high parton densities in the proton-proton collisions produced by LHC, quarkonium pairs can be produced in single parton scattering (SPS) or double parton scattering (DPS) processes. SPS is assumed to dominate and produces pairs of strongly correlated mesons with small rapidity difference, SPS leads to the production of multiple heavy flavour quarks and meson pairs with large rapidity difference [2, 3]. The quarkonium production mechanism involves the production of color-singlet states, that is dominant at low transverse momentum, and color-octet states that become more important at higher p_T [4, 5]. Another source of quarkonium pairs is the decay of tetra-quarks [6].

The selection of double- Υ events at CMS [7] required the reconstruction of muons with hits in the strip tracker and pixel detector and the match of the extrapolated track with at least one segment reconstructed in the muon chambers. Cuts on muon (dimuon) p_T and η (y) were then applied to select a region with an uniform acceptance: $p_{T,\mu} > 3.5 \text{ GeV}$, $|\eta_\mu| < 2.4$, $p_{T,\Upsilon} < 50 \text{ GeV}$, $|y_\Upsilon| < 2.0$. Events with multiple Υ were discarded and the production of non prompt pairs was neglected.

In the invariant mass distribution the yield of two $\Upsilon(1S)$ or a $\Upsilon(1S)$ and a $\Upsilon(2S)$ were estimated, while no visible signal appeared for $\Upsilon(3S)$. A two-dimensional fit was performed over the mass distribution, with five components corresponding to $\Upsilon(1S)\Upsilon(1S)$, $\Upsilon(1S)\Upsilon(2S)$ pairs, one $\Upsilon(1S)$ or $\Upsilon(2S)$ and one dimuon from combinatorial background and two combinatorial dimuons. The signal was described with a Crystal-Ball function and background with a Chebyshev polynomial; the fit result is shown in Fig. 1.

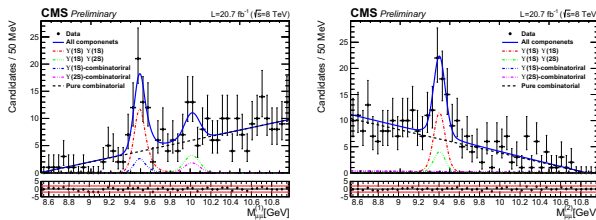


Figure 1. Projections of the 2D fit: invariant mass of higher mass muon pairs, $M_{\mu\mu}^{(1)}$ (left) and lower mass muon pairs, $M_{\mu\mu}^{(2)}$ (right). The lower pads show the difference between the total fit curve and data, with red lines corresponding to a difference of ± 2 standard deviations.

The cross section was extracted from the signal yield multiplying the number of fitted signal events n_{sig} for a correction factor $\bar{\omega}$, accounting for acceptance and efficiency, and dividing by the squared branching ratio of the Υ and the integrated luminosity:

$$\sigma_T = \frac{n_{\text{sig}} \cdot \bar{\omega}}{\mathcal{B}(\Upsilon(1S) \rightarrow \mu^+ \mu^-)^2 \cdot \mathcal{L}}$$

Acceptance and efficiency were computed event-by-event on a simulated sample assuming isotropic decays.

The total measured cross-section was [7]

$$\sigma_T = (68.8 \pm 12.7(\text{stat}) \pm 7.4(\text{syst}) \pm 2.8(\text{BR})) \text{ pb},$$

where the last systematic uncertainty comes from the $\Upsilon \rightarrow \mu^+ \mu^-$ branching ratio. Other systematic uncertainties were estimated by changing the functions used to describe signal and background, the estimation of acceptance and efficiency and the integrated luminosity. Υ polarization affects significantly the acceptance, that was estimated assuming unpolarized production: that was compared with the hypotheses of full longitudinal or transverse polarization showing a variation of -38% and +36%.

4 B^+ production

The measurement and study of beauty hadron production cross-section at high energies provide new important tests of theoretical calculations [8, 9]. The B^+ production cross-section was measured at the CMS experiment looking at the decay $B^+ \rightarrow J/\psi K^+$, followed by the decay $J/\psi \rightarrow \mu^+\mu^-$ [10]; charge conjugation states are implied here and in the following. The differential cross-section versus transverse momentum or rapidity was measured in a rapidity range $|y_B| < 2.4$ and transverse momentum range $10 \text{ GeV} < p_{T,B} < 100 \text{ GeV}$, using a subsample of data collected in 2015 corresponding to an integrated luminosity $\mathcal{L} = 50.8 \text{ pb}^{-1}$. The differential cross-section was extracted from the signal yield in each bin dividing by the branching ratios \mathcal{B} , acceptance A , efficiency ϵ , integrated luminosity and the bin width Δz , with $z = p_{T,B}, y_B$. An additional factor 2 was included to account for B charge symmetry, while the cross-section for the production of B^+ only was quoted:

$$\frac{d\sigma(pp \rightarrow B^+ X)}{dz} = \frac{n_{\text{sig}}(z)}{2 \cdot \mathcal{B} \cdot A \cdot \epsilon(z) \cdot \mathcal{L} \cdot \Delta z}.$$

Events were selected applying the requirements on muon quality as described in Sect. 3; candidate J/ψ mesons were reconstructed combining pairs of oppositely-charged muons having an invariant mass within $\pm 150 \text{ MeV}$ of the nominal J/ψ mass, $p_{T,J/\psi} > 8 \text{ GeV}$ and a χ^2 probability of the vertex-fit larger than 10%. Candidate B^+ mesons were reconstructed combining a J/ψ candidate with a charged track with $p_T > 1 \text{ GeV}$; the track was assumed to be a kaon and the track fit was required to give $\chi^2/n_{\text{d.o.f.}} < 5$. A kinematic fit was performed, constraining the dimuon mass to the nominal J/ψ mass; the three-track combination was required to be compatible with having a common vertex with a vertex-fit χ^2 probability larger than 10% and a reconstructed invariant mass $M_{J/\psi K}$ in the range $5 \div 6 \text{ GeV}$. The transverse decay distance divided by its uncertainty was required to exceed 3.5 and the cosine of the angle between B^+ candidate momentum and the vector formed by the interaction point and the $\mu\mu K$ vertex in the transverse plane had to be greater than 0.99.

The B^+ invariant mass distribution was built in bins of transverse momentum and an unbinned maximum likelihood fit was performed; the signal was described with the sum of two gaussians and the background with an exponential plus an error function to describe the contribution of mis-reconstructed decays of B^+ with additional particles in the final state. The invariant mass distribution for the inclusive sample in the total acceptance region is shown in Fig. 2.

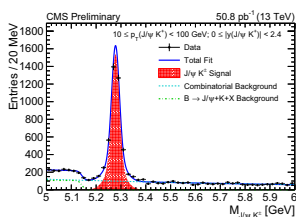


Figure 2. Invariant mass distribution of the full $B^\pm \rightarrow J/\psi K^\pm$ candidates sample: the solid curve shows the result of the fit, the shaded area represents the signal component, the dashed and dash-dotted curves represent the combinatorial and mis-reconstructed $B^\pm \rightarrow J/\psi K^\pm X$ background components, respectively.

The acceptance and efficiency were estimated with a sample of simulated events; trigger and muon reconstruction efficiency was estimated also in data selecting an inclusive J/ψ sample and applying a tag-and-probe method: the difference with the one obtained from the simulation was included in the systematic uncertainties.

To estimate other systematic uncertainties the mass modeling functions were changed; the rare decay $B^+ \rightarrow J/\psi \pi^+$ was included in the fit; the uncertainty coming from bin to bin migration of events, due to finite resolution, was estimated by examining the generator information in the simulated samples. Uncertainties associated to the $p_{T,B}$ and y_B distributions used in the generation were evaluated

with event-by-event weights determined from the differences between the distributions generated by PYTHIA and given by the FONLL calculations. The uncertainty on the B^+ lifetime was also included, the error on the integrated luminosity is 4.8% and the uncertainty on the branching ratios is 3.1%.

The differential cross-section versus transverse momentum and rapidity [10] is shown in Fig. 3, together with the results obtained at $\sqrt{s} = 7$ TeV [11] and the predictions from FONLL and PYTHIA [8, 12–14].

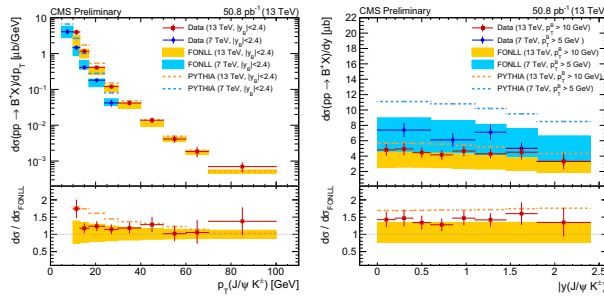


Figure 3. Differential cross-section versus transverse momentum (left) and rapidity (right), compared with predictions from FONLL (boxes) and PYTHIA (dashed lines). The lower pads display the data over FONLL cross section ratios (dots) and the PYTHIA/FONLL ratios (dashed lines).

5 Quarkonium production

Quarkonium production can be described in two phases, with a perturbative generation of a quark-antiquark pair in a singlet or octet state followed by the hadronization producing a bound state, described by a long-distance matrix element [15–18]. Measurements at different energies allow for a test of this factorization; predictions are done performing different perturbative calculations for each different collision energy and using the same matrix element at all energies [19, 20].

Higher energies, with higher cross-sections, allow for a measurement with an extended reach in transverse momentum, up to 120 GeV for rapidity up to 1.2, using the full available data sample collected in 2015 [21]. The product of double-differential cross-section by decay branching ratio was extracted from the signal yield in each bin dividing by acceptance A , efficiency ϵ , integrated luminosity and the bin widths:

$$\mathcal{B}(Q\bar{Q} \rightarrow \mu^+\mu^-) \cdot \frac{d^2\sigma(pp \rightarrow Q\bar{Q}X)}{dp_T dy} = \frac{N_{Q\bar{Q}}(z)}{\mathcal{L} \cdot \Delta p_T \Delta y} \cdot \left\langle \frac{1}{A(p_T, y) \cdot \epsilon(p_T, y)} \right\rangle.$$

The signal yield in each bin was extracted from an unbinned maximum likelihood fit; the signal was described with a Crystal Ball function and the background with an exponential.

Charmonia can be produced in primary proton-proton interactions (prompt) and b -hadron decays (non-prompt); the two components were separated performing a simultaneous fit to the invariant mass and the “pseudo-proper decay length” [22], with a function describing the prompt component with a resolution function, the non prompt component with an exponential convoluted with a resolution function, and the background with a gaussian plus an exponential.

In Fig. 4 the fits to the mass and pseudo-proper decay length are shown for J/ψ in a p_T, y bin.

Acceptance has been estimated in a generated event sample by looking at the fraction of generated events passing the selection; in the generation an unpolarized production of quarkonia has been assumed. Efficiency has been estimated with the tag-and-probe method.

Uncertainties related to the signal yield estimation have been evaluated by changing the parameters in the Crystal Ball function, leaving the masses free in the fit and changing the functions for the background. Uncertainties on the non-prompt fraction have been estimated by calculating the decay

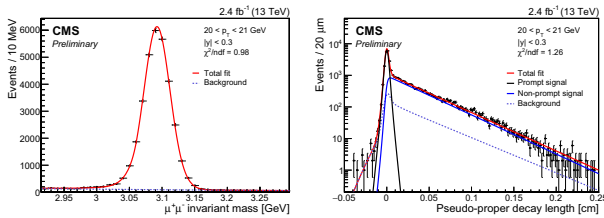


Figure 4. J/ψ fits: mass (left), pseudo-proper decay length (right).

length from the primary vertex in place of the average collision point, using different functions for the background or changing parameters constraints.

The double-differential cross-sections vs. p_T for different y bins are shown in Fig. 5 for J/ψ and $\psi(2S)$ and in Fig. 6 for $\Upsilon(1S)$, $\Upsilon(2S)$ and $\Upsilon(3S)$; the comparisons with the measurements at 7 TeV [23, 24] are shown in Fig. 7.

The non-prompt fractions versus p_T for J/ψ and $\psi(2S)$, compared with the corresponding measurements at 7 TeV [25], are shown in Fig. 8.

6 Conclusions

Differential cross section for B^+ production at $\sqrt{s} = 13$ TeV has been measured for p_T up to 100 GeV; a reasonable agreement with FONLL calculations and with PYTHIA has been found.

The double differential production cross sections at $\sqrt{s} = 13$ TeV for J/ψ , $\psi(2S)$, $\Upsilon(nS)$ has been measured. These results shall contribute to consolidate the underlying hypotheses of NRQCD and provide further input to constrain the theory parameters.

The simultaneous production of two $\Upsilon(1S)$ at $\sqrt{s} = 8$ TeV has been observed and the total cross-section has been measured.

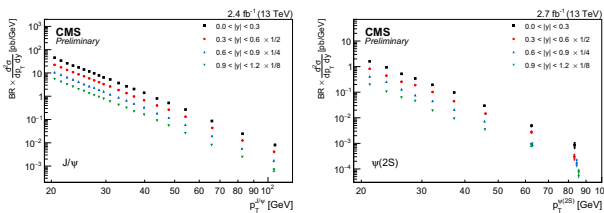


Figure 5. Double-differential cross-sections vs. p_T : J/ψ (left), $\psi(2S)$ (right).

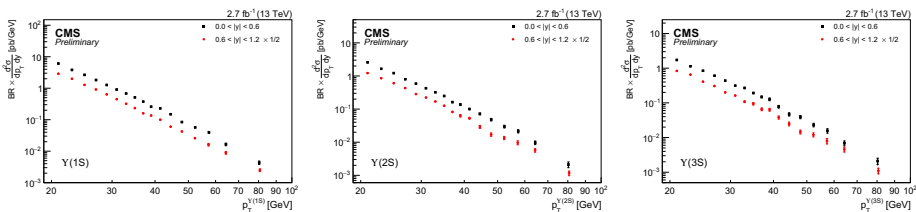


Figure 6. Double-differential cross-sections vs. p_T : $\Upsilon(1S)$ (left), $\Upsilon(2S)$ (middle), $\Upsilon(3S)$ (right).

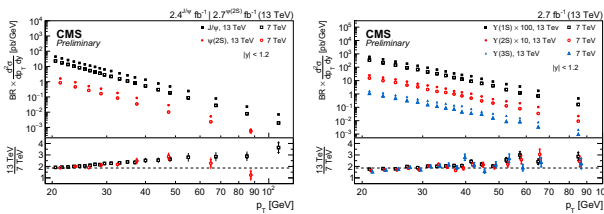


Figure 7. Comparison of the double-differential cross-sections vs. p_T for 13 TeV and 7 TeV: J/ψ and $\psi(2S)$ (left), $Y(1S)$, $Y(2S)$ and $Y(3S)$ (right). The lower pads display the cross section ratios.

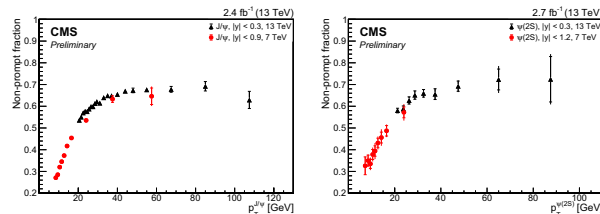


Figure 8. Comparison of the non-prompt fraction of J/ψ (left) and $\psi(2S)$ (right) as a function of p_T for 13 TeV and 7 TeV.

References

- [1] CMS Collaboration, *J. Inst.* **03**, S08004 (2008)
- [2] S.P. Baranov *et al.*, *Phys. Lett. B* **705**, 116 (2011)
- [3] C.H. Kom *et al.*, *Phys. Rev. Lett.* **107**, 082002 (2011)
- [4] P. Ko *et al.*, *J. High Energy Phys.* **01**, 070 (2011)
- [5] J. Campbell *et al.*, *Phys. Rev. Lett.* **98**, 252002 (2007)
- [6] A.V. Berezhnoy *et al.*, *Phys. Rev. D* **86**, 034004 (2012)
- [7] CMS Collaboration, CMS-PAS-BPH-14-008 (2016)
- [8] M. Cacciari *et al.*, *J. High Energy Phys.* **05**, 007 (1998)
- [9] B.A. Kniehl *et al.*, *Phys. Rev. D* **77**, 014011 (2008)
- [10] CMS Collaboration, CMS-PAS-BPH-15-004 (2016)
- [11] CMS Collaboration, *Phys. Rev. Lett.* **106**, 112001 (2011)
- [12] M. Cacciari *et al.*, *J. High Energy Phys.* **03**, 006 (2001)
- [13] M. Cacciari *et al.*, *J. High Energy Phys.* **10**, 137 (2012)
- [14] M. Cacciari *et al.*, arXiv:1507.06197 (2015)
- [15] G.T. Bodwin *et al.*, *Phys. Rev. D* **51**, 1125 (1995)
- [16] G.T. Bodwin *et al.*, *Phys. Rev. D* **55**, 5853 (1997)
- [17] P.Cho and A.K.Leibovich, *Phys. Rev. D* **53**, 150 (1996)
- [18] P.Cho and A.K.Leibovich, *Phys. Rev. D* **53**, 6203 (1996)
- [19] P. Faccioli *et al.*, *Phys. Lett. B* **736**, 98 (2014)
- [20] G.T. Bodwin *et al.*, *Phys. Rev. Lett.* **113**, 022001 (2014)
- [21] CMS Collaboration, CMS-PAS-BPH-15-004 (2016)
- [22] CMS Collaboration, *Eur. Phys. J. C* **71**, 1575 (2011)
- [23] CMS Collaboration, *Phys. Rev. Lett.* **114**, 191802 (2015)
- [24] CMS Collaboration, *Phys. Lett. B* **749**, 14 (2015)
- [25] CMS Collaboration, *J. High Energy Phys.* **02**, 011 (2012)